Chinese Journal of Catalysis 41 (2020) 877–888

available at www.sciencedirect.com

ScienceDirect

journal homepage: www.elsevier.com/locate/chnjc

Article

Investigation of lattice capacity effect on Cu^{2+}-doped SnO_2 solid solution catalysts to promote reaction performance toward NO_x-SCR with NH_3

Xianglan Xu [a], Yunyan Tong [a], Jingyan Zhang [a], Xiuzhong Fang [a], Junwei Xu [a], Fuyan Liu [a], Jianjun Liu [b], Wei Zhong [c], Olga E. Lebedeva [d], Xiang Wang [a,*]

[a] *Key Laboratory of Jiangxi Province for Environment and Energy Catalysis, College of Chemistry, Nanchang University, Nanchang 330031, Jiangxi, China*
[b] *Jiangxi Baoan New Material Technology Corporation, LTD, Pingxiang 337000, Jiangxi, China*
[c] *College of Biological, Chemical Sciences and Engineering, Jiaxing University, Jiaxing 314001, Zhejiang, China*
[d] *Belgorod State National Research University, Pobeda Str., 85 Belgorod, 308015, Russian Federation*

ARTICLE INFO

Article history:
Received 13 November 2019
Accepted 10 December 2019
Published 5 May 2020

Keywords:
SnO_2-based solid solution
Lattice capacity of Cu^{2+}
XRD extrapolation method
NO_x-SCR with NH_3
Threshold effect

ABSTRACT

To understand the effect of the doping amount of Cu^{2+} on the structure and reactivity of SnO_2 in NO_x-SCR with NH_3, a series of Sn-Cu-O binary oxide catalysts with different Sn/Cu ratios have been prepared and thoroughly characterized. Using the XRD extrapolation method, the SnO_2 lattice capacity for Cu^{2+} cations is determined at 0.10 g CuO per g of SnO_2, equaling a Sn/Cu molar ratio of 84/16. Therefore, in a tetragonal rutile SnO_2 lattice, only a maximum of 16% of the Sn^{4+} cations can be replaced by Cu^{2+} to form a stable solid solution structure. If the Cu content is higher, CuO will form on the catalyst surface, which has a negative effect on the reaction performance. For samples in a pure solid solution phase, the number of surface defects increase with increasing Cu content until it reaches the lattice capacity, as confirmed by Raman spectroscopy. As a result, the amounts of both active oxygen species and acidic sites on the surface, which critically determine the reaction performance, also increase and reach the maximum level for the catalyst with a Cu content close to the lattice capacity. A distinct lattice capacity threshold effect on the structure and reactivity of Sn-Cu binary oxide catalysts has been observed. A Sn-Cu catalyst with the best reaction performance can be obtained by doping the SnO_2 matrix with the lattice capacity amount of Cu^{2+}.

1. Introduction

Nitrogen oxides (NO_x) emitted from various processes are harmful to the atmosphere and human health. Several technologies have therefore been developed for NO_x elimination so far [1]. Among them, NO_x-SCR with NH_3 is an effective way to remove NO_x from both stationary plants and diesel engines [2–5]. In the context of practical applications, developing low-cost catalysts that offer high NO_x conversion and N_2 selectivity at both low and high temperatures and resist sulfur deactivation

* Corresponding author. E-mail: xwang23@ncu.edu.cn
This work was supported by the National Natural Science Foundation of China (21567016, 21666020, 21962009), the Natural Science Foundation of Jiangxi Province (20181ACB20005, 20171BAB213013), the Key Laboratory Foundation of Jiangxi Province for Environment and Energy Catalysis (20181BCD40004), National Key Research and Development Program of China (2016YFC0209302), the Innovation Fund Designated for Graduate Students of Jiangxi Province (YC2018-B015) and Natural Science Foundation of Zhejiang Province (LY18B010007),
DOI: 10.1016/S1872-2067(20)63532-X | http://www.sciencedirect.com/science/journal/18722067 | Chin. J. Catal., Vol. 41, No. 5, May 2020

are desirable. Compared with the extensively investigated supported catalytic materials based on precious metals and zeolites, base metal oxide catalysts have some apparent advantages, such as their abundant sources, low cost, and easy preparation. Therefore, NO_x-SCR catalysts based on non-noble-metal oxides have attracted much attention over the past several decades [6–9].

Metal oxide solid solutions exhibit some unique properties. In comparison with the corresponding individual components, they generally show improved physical chemical properties, which improves the catalytic performance for a variety of reactions [10–14]. For instance, with the formation of a solid solution structure, the thermal stability, surface areas, porous structure, and number of surface active oxygen sites can be significantly improved due to lattice distortion and the generation of lattice defects, which usually benefits the catalytic performance [14,15]. A representative case is that of Ce–Zr–O solid solutions, which have been industrialized on a large scale as oxygen storage components in three-way catalysts that control emissions from cars. Compared with the case of pure CeO_2, incorporation of Zr cations into the lattice of cubic flourite CeO_2 to form a stable solid solution structure remarkably improves the thermal stability as well as the oxygen storage capacity [16,17]. Numerous studies have also demonstrated that a solid solution catalyst often displays improved activity and stability than those of the individual metal oxides [18,19]. Therefore, a metal oxide solid solution acts as a principal heterogeneous catalyst, and such systems have been investigated extensively and intensively for different reactions.

Over the past 8 years, using SnO_2 as a model solvent metal oxide, we have systematically investigated the dissolution behavior of several metal cations in the lattice matrix of tetragonal rutile SnO_2 to form solid solution catalysts for various reactions [20–24]. In addition to evident changes in the texture and physical property, doping the secondary cations into SnO_2 lattice to form non-continuous solid solutions also increased the number of surface deficient oxygen sites on SnO_2, which could also be stabilized even at temperatures higher than 400 °C [20,22,23]. Moreover, due to the expanded surface area, Sn^{4+} cations enrich the catalysts' surfaces, thus increasing their Lewis acidity [24]. As a consequence, the activity of the prepared solid solution catalysts increased for different reactions [21]. Due to the difference in the metal cation radius and the initial crystalline phases, we noticed that lattice cations of the solvent metal oxide could be replaced by solute cations up to a certain extent. To define the maximum number of solute cations doped into the lattice of a solvent metal oxide to form a stable solid solution, the concept of lattice capacity has been established in our former report [22,23]. The lattice capacity might eventually influence the reaction performance of the catalysts. To gain a deeper understanding of the structure-reactivity relationship of solid solution catalysts, we have developed an easy XRD extrapolation method to quantify the lattice capacity of a solute cation in the lattice of a solvent metal oxide for non-continuous solid solutions [22,23].

We have recently demonstrated that SnO_2-based solid solutions modified by metal cations possessing redox ability (Ce^{4+} and Cu^{2+}) or acidity (In^{3+} and W^{6+}) exhibited improved reaction performance in NO_x-SCR with NH_3 compared to pure SnO_2 alone, due to the increased number of both surface active oxygen sites and enhanced acidity [24]. Although the Cu^{2+}-SnO_2 solid solution catalyst displays a slightly lower maximum NO_x conversion than the Ce^{4+}-SnO_2 catalyst, it shows a much higher low-temperature activity (below 250 °C). Thus, to prepare catalysts with better performance at both low and high temperatures, the Cu^{2+}-doped SnO_2 solid solution needs to be studied in greater detail. Therefore, with the objective to understand the effect of the doping amount of Cu^{2+} on the structure of SnO_2 and the reactivity, a series Sn–Cu–O binary oxide catalysts containing different amounts of Cu^{2+} have been prepared by the co-precipitation method. The SnO_2 lattice capacity for Cu^{2+} cations has been measured using the XRD extrapolation method [22,23]. Using different techniques, evolution of the structure, existing states of Cu and changes in the bulk/surface property of the prepared catalysts with the doping amount of Cu^{2+} cations have been explored and correlated with the reaction performance of the catalysts. The Cu^{2+}-doped SnO_2 solid solution catalyst displays an obvious threshold effect toward NO_x-SCR with NH_3, for which the catalyst possessing Cu^{2+} at an amount close to the lattice capacity exhibits optimal reaction performance.

2. Experimental

2.1. Catalyst preparation

All the chemicals were purchased from reliable commercialized sources and used without purification. $SnCl_4{\cdot}5H_2O$ (AR) was purchased from Sinopharm Chemical Reagent Co., Ltd. (Shanghai, China). Aqueous ammonia solution was supplied by Xilong Chemical Company (Guangdong, China). $Cu(NO_3)_2{\cdot}3H_2O$ (AR) was provided by Tianjing Chemical Company (Tianjing, China).

A series of Sn–Cu binary oxide catalysts with different Sn/Cu molar ratios was prepared by a traditional coprecipitation method. A calculated amount of $SnCl_4$ (0.5 mol L^{-1}) was mixed with a $Cu(NO_3)_2$ solution (0.5 mol L^{-1}) and stirred 2 h at ambient temperature to obtain a homogeneous solution. Under continuous stirring, an aqueous ammonia solution (25–28 wt%) was then added dropwise into the solution until the pH reached ~8.0, and the solution was then stirred for another 10 h, which was followed by centrifugation. The precipitates were washed with distilled deionized water until the filtrate was free of Cl^-, which was indicated by a TDS of less than 0.002%. The obtained solids were dried at 110 °C for 12 h and calcined at 550 °C in air for 4 h, subjected to a heating ramp of 2 °C min^{-1}, to obtain the final catalysts. The catalysts were named SnCux–y, according to the Sn/Cu molar ratio. For example, SnCu9–1 represents a catalyst with a Sn/Cu molar ratio of 9/1. The elemental compositions of the catalysts were confirmed by ICP to correspond to the original ratios used in sample preparation within the bounds of experimental error, as shown in Table 1. For comparison, pure SnO_2 and CuO samples were prepared by the same procedure.

Table 1
XRD results for the catalysts.

Catalyst	Sn/M molar ratio by ICP	I/I_0 [a]	Phase composition	Lattice parameters			Cell volume [c] (Å^3)	Average crystallite size [d] (nm)
				$a = b$ (Å)	c (Å)	$\alpha/\beta/\gamma$ (°)		
SnO_2	—	—	SnO_2	4.733	3.156	90	70.70	9.8
SnCu9.5–0.5	9.5/0.5	0.000	SS [b]	4.733	3.169	90	70.99	7.2
SnCu9–1	9.0/1.0	0.000	SS	4.735	3.183	90	71.36	5.8
SnCu8.5–1.5	8.5/1.5	0.000	SS	4.738	3.185	90	71.50	6.0
SnCu8–2	7.9/2.1	0.160	SS, CuO	4.740	3.187	90	71.61	6.1
SnCu7–3	7.0/3.0	0.343	SS, CuO	4.740	3.187	90	71.61	7.3
SnCu6–4	6.1/3.9	0.537	SS, CuO	4.740	3.187	90	71.61	7.9
SnCu5–5	5.5/4.5	0.712	SS, CuO	4.740	3.187	90	71.61	7.9
SnCu4–6	4.5/5.5	1.502	SS, CuO	4.740	3.187	90	71.61	6.6

[a] Ratio of peak intensity of CuO (11-1) at 35.61° to that of SnO_2 (110) at 26.82° in Fig. 1(a).
[b] SS: SnO_2 solid solution phase.
[c] Cell volume = $a \times a \times c$.
[d] Calculated by Scherrer's equation with XRD (110) peak of SnO_2.

2.2. Catalyst characterization

Powder X-ray diffraction (XRD) patterns were recorded on a Bruker AXS D8FOCus diffractometer operating at 40 kV and 30 mA with Cu K_α irradiation (λ = 1.5405 Å). Scans were taken with a 2θ range of 10°–90° and a step of 2° min^{-1}. The calculated experimental error for 2θ measurements of the peaks was ± 0.01°. The mean crystalline sizes of the SnO_2 particles were calculated using Scherrer's equation employing the diffraction peak corresponding to the SnO_2 (110) facet.

Raman spectra of the catalysts were recorded using a Renishaw inVia instrument with an excitation wavelength of 532 nm, and the measured Raman shift ranged between 400 and 900 cm^{-1}.

Inductively coupled plasma optical emission spectroscopy (ICP-OES) experiments were conducted on a VARIAN ICP-715ES instrument to verify the elemental compositions of the catalysts.

N_2 adsorption-desorption experiments were performed at –196 °C to determine the textural properties of catalysts on a Micromeritics ASAP 2020 system. Before the measurement, the catalyst was subjected to vacuum at 250 °C for 4 h. The specific surface area of the catalyst was obtained using the BET method in the relative pressure range of p/p_0 = 0.05–0.25. The pore size distribution was acquired employing the Barrett-Joyner-Halenda (BJH) method. The mean pore size was obtained from the corresponding distribution curve. The pore volume was calculated to be p/p_0 = 0.99.

Hydrogen temperature-programmed reduction (H_2-TPR) experiments were conducted on a FINESORB 3010C instrument to analyze the reduction behavior of catalysts. Typically, 10 mg of the catalyst was used for the test. Prior to the experiment, the catalyst was pre-treated at 120 °C for 30 min under a 30 mL min^{-1} high-purity Ar flow to remove any surface impurities. After cooling to room temperature, the catalyst was then heated in a 30 mL min^{-1} 10% H_2/Ar flow to 900 °C at a rate of 10 °C min^{-1}. A thermal conductivity detector (TCD) was used to measure the H_2 uptake. For quantification, a CuO (99.99%) standard sample was used to calibrate the system.

Oxygen temperature-programmed desorption (O_2-TPD) experiments were performed on a DAS-7000 system. Typically, 50 mg of the catalyst was placed in a quartz reactor, pretreated in ultrahigh-purity (UHP) Ar flow at 400 °C for 30 min. After cooling to 50 °C, the catalyst was then saturated under a 30 mL min^{-1} pure oxygen flow at the same temperature for 1 h. Afterwards, the catalyst was purged using a 30 mL min^{-1} UHP He flow for 30 min to remove any physically adsorbed O_2. O_2-TPD was then performed from 50 to 700 °C with a heating rate of 10 °C min^{-1} under a 30 mL min^{-1} UHP Ar flow. A TCD was used to record the signals.

NH_3 temperature-programmed desorption (NH_3-TPD) was conducted using a DAS-7000 system to investigate the acidic sites of the catalysts. In a typical test, 50 mg of the catalyst was loaded in a quartz tube. The catalyst was first pretreated at 400 °C under a UHP Ar flow with a flow rate of 30 mL min^{-1} for 1 h, and then cooled to 100 °C. At the same temperature, the catalyst was saturated in a 0.5% NH_3/Ar flow 30 mL min^{-1} for 1 h. Afterwards, the catalyst was flushed using a UHP Ar flow with a flow rate of 30 mL min^{-1} for 30 min. Subsequently, the catalyst was heated from 100 to 700 °C at a ramping rate of 10 °C min^{-1} in the same flow, with the NH_3 desorption amount being monitored by a TCD.

2.3. Catalytic performance evaluation

The reaction performance of NO_x-SCR with NH_3 on the catalyst was evaluated using a fixed-bed horizontal straight quartz reactor using 50 mg of the catalyst. The reaction feed consisted of 5% O_2, 0.05% NO, and 0.05% NH_3 with Ar balance gas. The total flow rate was 50 mL min^{-1}, corresponding to a total weight hourly space velocity (WHSV) of 60000 mL h^{-1} g_{cat}^{-1}. A thermocouple with its head point touching the catalyst was used to monitor the reaction temperature. Kinetic data were obtained by increasing the reaction temperature at 50 °C intervals. An online SHP8400 PMS gas mass spectrometer was used to analyze the products. To obtain steady-state kinetic data, the reaction was stabilized for 30 min at a certain temperature before an injection. The NO_x conversion was calculated by the following equation:

$$NO_x \text{ Conversion} = \frac{[NO_x]_{in} - [NO_x]_{out}}{[NO_x]_{in}} \times 100\%.$$

$[NO_x]_{in}$ and $[NO_x]_{out}$ represent the NO_x concentrations in the inlet and outlet gas feed, respectively. The N_2 and N_2O concentrations in the outlet gas flow were directly quantified using mass spectrometry.

3. Results and discussion

3.1. XRD measurement for phase compositions of catalysts

To determine the phase compositions of the catalysts, XRD experiments were performed. As shown in Fig. 1(a), the three strongest peaks of pure SnO_2 were observed at 2θ values of 26.82°, 34.03° and 51.94°, corresponding to the (110), (101), and (211) facets, respectively, which are typical for the tetragonal rutile SnO_2 (PDF-ICDD 41–1445) crystalline phase [15]. For CuO, the three strongest peaks were observed at 2θ values of 35.61°, 38.77° and 48.82°, corresponding to the (11-1), (111), and (20-2) facets, respectively, which are characteristic for the monoclinic CuO (JCPDS NO. 48–1548) crystalline phase [20]. The sharp diffraction peaks indicate that both of the pure oxides crystallized well after calcination. For clarification, the observed phase compositions of the catalysts with different Sn/Cu ratios are listed in Table 1.

For Sn-rich Sn–Cu binary oxide catalysts with Sn/Cu molar ratios above 8/2, only the evidently broadened SnO_2 diffraction peaks could be detected, indicating that Cu^{2+} cations could have entered the SnO_2 lattice matrix to form a solid solution structure, thus escaping detection by XRD and impeding crystallization of the Sn–Cu oxide catalysts [22,23]. However, when the Sn/Cu molar ratios reached 8/2, microcrystalline CuO particles started to appear, whose intensity increased with increasing Cu content, as demonstrated by the distinct CuO (11-1) diffraction peak at 35.61°. This proves that the amount of surface CuO crystalline phase increased, resulting in growth of the CuO crystallite.

As discussed in our previous report [22,23], for a non-continuous solid solution, the solute cations usually dissolve in the lattice of a solvent metal oxide up to a certain extent, which is termed the lattice capacity, which can be easily quantified by an XRD extrapolation method developed by our group. SnO_2, the solvent metal oxide used in this study, has a tetragonal rutile crystalline structure, wherein Sn^{4+} has a coordination number (CN) of 6 and a radius of 0.69 Å. If a Cu^{2+} cation dissolves in the crystalline matrix of SnO_2 to form a solid solution structure, it should also have a CN of 6, resulting in a radius of 0.73 Å. According to the rules of solid solution formation [25,26], it is highly likely for Cu^{2+} cations to dissolve in the SnO_2 lattice matrix to form a substitution solid solution with a certain lattice capacity. Indeed, our previous studies have proven that Cu^{2+} cations can dissolve in the lattice matrix of SnO_2 with different morphologies when its content is low [20,24].

The mean crystallite sizes of SnO_2 in the catalysts were calculated and have been listed in Table 1. Apparently, SnO_2 phases in the Sn–Cu oxide catalysts had smaller crystallites than those of pure SnO_2, which further suggested that Cu^{2+} cations might have dissolved in the SnO_2 lattice matrix to form a solid solution structure, thereby hampering the crystallization of the SnO_2 phase during calcination.

To better understand the structure–reactivity relationship of the Sn–Cu solid solution catalysts, the lattice capacity of SnO_2 for Cu^{2+} cations was quantified by the XRD extrapolation method [22,23], as shown in the correlation diagram displayed in Fig. 1(b). Considering the formation of a non-continuous solid solution, e.g., the formation of a Cu^{2+}-doped SnO_2 solid solution, Cu^{2+} cations will first partially substitute the Sn^{4+} cations and get embedded in the lattice matrix of SnO_2; thus, XRD could not detect a CuO phase. After its content reached the lattice capacity, polymeric and amorphous CuO species will start to form on the catalyst surface. However, unless the CuO crystallites reach a certain size (approx. 2–3 nm) [27], the CuO phase would not be observed by XRD. Therefore, the lattice capacity can only be extrapolated by the correlated line shown in Fig. 1(b). Theoretically, the amount of crystalline CuO is intimately related to the total Cu content in the Sn–Cu binary oxide catalysts, and the intensity of its diffraction peaks reflects the amount of the CuO crystalline phase. In this study, the intensity (I) of CuO (11-1), which showed the strongest peak for the CuO crystalline phase, was used to measure the amount of crystalline CuO formed in each catalyst. To eliminate the possibility of any factor influencing the absolute peak intensity, for example, the color change of the sample on X-ray absorption, the intensity (I_0) of the strongest peak of SnO_2 (110) was used to normalize I to get a series of I/I_0 ratios (Table 1), which cor-

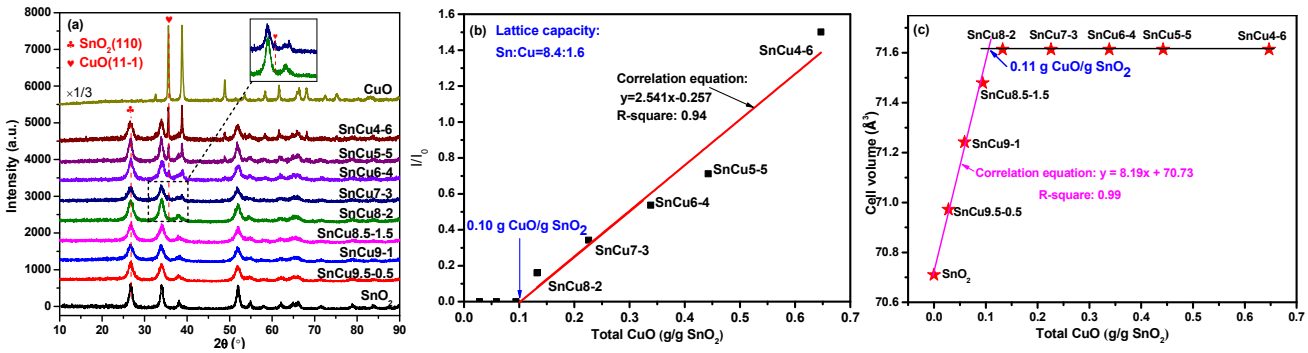

Fig. 1. XRD results obtained for Sn-Cu oxide catalysts. XRD patterns (a) and lattice capacity (b) of SnO_2 for Cu^{2+} cations; (c) Change in SnO_2 cell volume against CuO content.

relate to the amount of CuO crystalline phase in the samples. The I/I_0 ratios were then plotted against the CuO amount in the samples, which was normalized by the SnO_2 content in each sample. As exhibited in Fig. 1(b), a correlated line was obtained, which intersects the x axis at 0.10 g CuO per g SnO_2. This corresponds to the extrapolated lattice capacity, which equals a Sn/Cu molar ratio of 84/16. In other words, in the lattice matrix of rutile SnO_2, only a maximum of 16% of the Sn^{4+} cations can be replaced by Cu^{2+} cations to form a stable solid solution structure. When the Cu^{2+} cation content is above this capacity, the excess Cu^{2+} cations will form free CuO species on the solid solution surface. When the size of the CuO microcrystallites reached about 3 nm, they could be detected by XRD, and its diffraction intensity increased with the amount of Cu, as observed in Fig. 1(a) and (b). Notably, for SnCu9.5–0.5, SnCu9–1, and SnCu8.5–1.5, since the Cu content was still below the lattice capacity, all the Cu^{2+} cations were embedded in the lattice matrix of SnO_2, thus escaping detection by XRD.

To verify the accuracy of the lattice capacity of Cu^{2+} cations in SnO_2 lattice determined by the XRD extrapolation method, the lattice parameters and cell volumes of the SnO_2 phases in the catalysts were calculated, as listed in Table 1. The lattice parameters of all the catalysts were in accordance with the tetragonal rutile structure of SnO_2. However, in comparison with the pure SnO_2 sample, the side lengths and cell volumes of the SnO_2 unit cell kept increasing with increase in the Cu content for the Sn–Cu binary samples until the Sn/Cu molar ratio reached 8/2. As discussed above, the radius of a Cu^{2+} cation is larger than that of Sn^{4+} when they have the same CN of 6. The increase in the side lengths and cell volume indeed provided additional evidence of the Cu^{2+} cations entering the lattice of tetragonal SnO_2 below this Sn/Cu molar ratio. Interestingly, further increasing the Cu content did not clearly affect the lattice parameters any more, indicating that after the Cu amount is above the lattice capacity, the excess Cu will form CuO species on the catalyst surface instead of staying in the SnO_2 lattice matrix.

The cell volume of the SnO_2 phase for each sample was then plotted against the CuO content in the samples. As depicted in Fig. 1(c), two correlated linear plots were obtained, which crossed each other at a turning point corresponding to 0.10 g CuO/g SnO_2. This is the same as the value obtained by the XRD extrapolation method. The results indicate that when the Cu^{2+} content is below the lattice capacity, the lattice parameters of SnO_2 indeed maintain a linear correlation with the Cu^{2+} content, which is consistent with Vegard's Law [28]. In contrast, once the Cu^{2+} content is above the lattice capacity, the lattice parameters of SnO_2 remain unchanged because no extra Cu^{2+} cation can be dissolved in the lattice matrix of SnO_2 anymore. In summary, the cell volume change results were consistent with the lattice capacity obtained by the XRD extrapolation method within the bounds of experimental error, confirming that the lattice capacity of Cu^{2+} cation in the SnO_2 lattice is 0.10 g CuO/g SnO_2, which equals a Sn/Cu molar ratio of 84/16. To form a stable non-continuous Sn–Cu solid solution, only 16% of the Sn^{4+} cations can be replaced by Cu^{2+} cations.

3.2. Raman analysis of catalysts

The Raman spectra of all the catalysts are shown in Fig. 2. Pure SnO_2 shows the strongest and typical A_{1g} peak at 633 cm^{-1} along with five weaker E_g, $2A_{2u}$, B_{1u}, and B_{2g} peaks [29,30], in which A_{1g} and B_{2g} are related to the expansion and contraction of Sn–O bonds in the plane perpendicular to the c axis [31]. Pure CuO exhibits only a weak B_g peak at 614 cm^{-1} [32], assigned to the symmetric oxygen stretching mode [33]. For SnCu9.5–0.5, SnCu9–1, and SnCu8.5–1.5 catalysts, which had Cu contents below the lattice capacity, similar Raman spectra as that of pure SnO_2 were obtained. However, the peaks show a red shift with increase in the Cu content, as demonstrated by the strongest A_{1g} peak of SnO_2 shifting from 628 to 618 cm^{-1} in these three catalysts in comparison with 633 cm^{-1} for pure SnO_2. The red shift can be attributed to changes in the SnO_2 lattice parameter and the presence of oxygen vacancies due to the formation of a SnO_2 solid solution structure [34]. In contrast, starting from SnCu8–2, the catalysts with Cu contents just above the lattice capacity, the strongest A_{1g} peak of SnO_2 are located at ~614 cm^{-1} and remain unchanged on further increasing the Cu content, which overlaps the typical E_g peak of CuO. In SnCu8–2, SnCu7–3, and SnCu6–4, we believe that the SnO_2 species still dominates the catalyst surface since the Raman band at 614 cm^{-1} is much stronger than that of the pure CuO sample. However, in SnCu5–5 and SnCu4–6, highly dispersed CuO should dominate the catalyst surface and cover the signal from SnO_2, as indicated by the very weak 614 cm^{-1} band similar to that of the E_g peak of CuO. This provides additional evidence suggesting that no extra Cu^{2+} cation can be doped into the SnO_2 lattice if the Cu content exceeds the lattice capacity of SnO_2 for Cu^{2+} cations, but the cations instead form highly dispersed CuO species on the catalyst surface. In addition, as listed in Table 2, the Raman peaks of Sn–Cu oxide catalysts obviously broadened, as demonstrated by the larger half width of the strongest A_{1g} peak in comparison with that of pure SnO_2. The broadening of the A_{1g} peak reflects the decrease in the size of the particles, which is consistent with the XRD results [30].

According to formerly published literature [30], the B_{1u} peak at ~550 cm^{-1} (labeled as α) and A_{2u} peak at ~681 cm^{-1} (labeled as β) are related to the lattice disorder and surface defects of

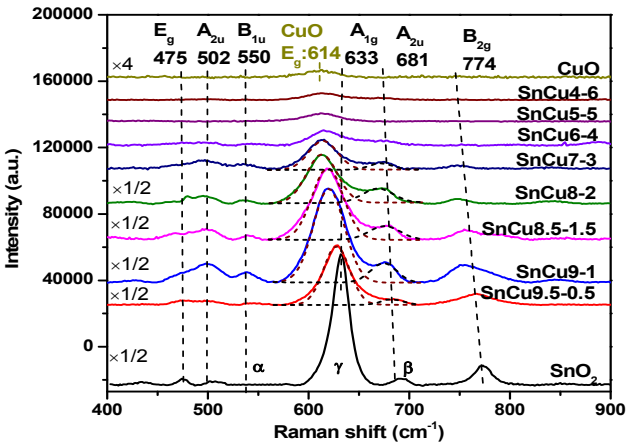

Fig. 2. Raman spectra of the Sn–Cu oxide catalysts.

Table 2
Raman results for the catalysts.

Catalyst	Raman Shift of A_{1g} peak (cm^{-1})	FWHM of Raman line (cm^{-1})	Integrated peak areas (a.u.)			(α+β)/γ
			α peak	β peak	γ peak	
SnO_2	633	19.5	—	2.8	89.1	0.03
SnCu9.5–0.5	628	29.3	0.8	2.9	61.9	0.06
SnCu9–1	619	37.8	5.7	9.1	100.0	0.15
SnCu8.5–1.5	618	35.3	4.2	8.0	76.5	0.16
SnCu8–2	614	28.2	3.5	5.2	71.4	0.12
SnCu7–3	614	34.1	1.1	1.4	37.1	0.07
SnCu6–4	615	34.4	0.5	1.0	21.9	0.07
SnCu5–5	615	40.2	—	0.5	22.1	0.02
SnCu4–6	614	41.1	—	0.4	22.3	0.02
CuO	614 [a]	31.3	—	—	—	—

[a] Raman shift of E_g peak of CuO.

SnO_2, which might correspond to SnO_2 lattice and surface oxygen vacancies. Therefore, the value of the sum of the integrated areas of B_{1u} and A_{2u} peaks divided by the integrated area of the A_{1g} peak (labeled as γ), i.e., the ratio (α + β)/γ, was determined to estimate the oxygen vacancy concentration on the catalysts. As shown in Table 2, it was apparent that the (α+β)/γ ratios of SnCu9.5–0.5, SnCu9–1, and SnCu8.5–1.5, i.e., the catalysts possessing the pure solid solution phase, increased with increasing Cu content. This demonstrates that, when Cu^{2+} cations enter the SnO_2 lattice to form a solid solution structure, more lattice and surface vacancies can be created. However, when the Cu content is over the lattice capacity, the excess Cu will form CuO on the catalyst surface, which is not beneficial but detrimental to the formation of surface vacancies, as evidenced by the decreasing (α+β)/γ ratios starting from the SnCu8–2 sample.

In brief, the Raman results confirmed the XRD results, showing that the incorporation of Cu^{2+} into the SnO_2 lattice has an evident lattice capacity threshold effect. When the Cu content is below the lattice capacity to form a pure phase solid solution structure, the number of surface vacancies increases with increasing Cu content. As a result, SnCu8.5–1.5, which has a Cu content close to the lattice capacity, possessed the largest number of surface vacancies among all the Sn–Cu oxide catalysts investigated.

3.3. N_2 sorption analysis of catalysts

The textural properties of the catalysts were analyzed by the N_2 adsorption–desorption technique. As displayed in Fig. S1(a), pure CuO showed a very small amount of N_2 sorption with a type-IV isotherm and H3-type hysteresis loop, implying that it was non-porous with a very small pore volume and surface area (Table 3). In contrast, individual SnO_2 presents an evident type-IV isotherm with an H2-type hysteresis loop, which is typical of mesoporous materials. Notably, all the Sn–Cu binary oxide catalysts possessed textural properties similar to those of SnO_2. However, Fig. S1(b) demonstrates that their pore distribution was obviously narrower than that of pure SnO_2, especially for those samples with Cu contents below or close to the lattice capacity. This testifies that the Cu^{2+} cations introduced into the SnO_2 lattice can alter the microstructure of the prepared samples, with the formation of a larger number of pores with smaller mean pore sizes, as shown in Table 3. While the average pore volumes of the Sn–Cu oxide catalysts showed no significant change, their specific surface areas increased evidently in comparison with that of SnO_2, in line with the results obtained for XRD crystallite size measurements and Raman analyses, demonstrating their improved thermal stability. Notably, SnCu9–1 and SnCu8.5–1.5, the catalysts with considerable numbers of lattice Cu^{2+} cations that retained the pure solid solution phase, exhibited much higher surface areas than that of individual SnO_2, demonstrating that the incorporation of Cu^{2+} cations can significantly restrict crystallization of the catalysts during calcination.

3.4. Reaction performance of catalysts

The reaction performance of all the catalysts for NO_x-SCR with NH_3 was evaluated, with the results shown in Fig. 3. As seen in Fig. 3(a), pure SnO_2 exhibited significant NO_x reduction activity due to the coexistence of both surface active oxygen and acidic sites [11,24,35], with the highest NO_x conversion of 40% achieved at 400 °C. In contrast, pure CuO showed obviously better activity at a much lower temperature, and offered the highest NO_x conversion of ~40% at 250 °C. It was noted that, for all the catalysts, N_2 was the predominant product and N_2O was produced as a negligible byproduct at different temperatures.

Interestingly, all the Sn–Cu binary catalysts displayed a better reaction performance than that offered by the two individu-

Table 3
N_2 sorption results for the catalysts.

Catalyst	Surface area [a] ($m^2 g^{-1}$)	Mean pore size [b] (nm)	Mean pore volume ($cm^3 g^{-1}$)
SnO_2	23	9.7	0.08
SnCu9.5–0.5	44	5.5	0.09
SnCu9–1	59	4.2	0.09
SnCu8.5–1.5	52	5.2	0.10
SnCu8–2	46	4.9	0.08
SnCu7–3	38	6.7	0.09
SnCu5–5	36	12.0	0.16
CuO	2	18.1	0.01

[a] Calculated by BET method.
[b] Determined by BJH method.

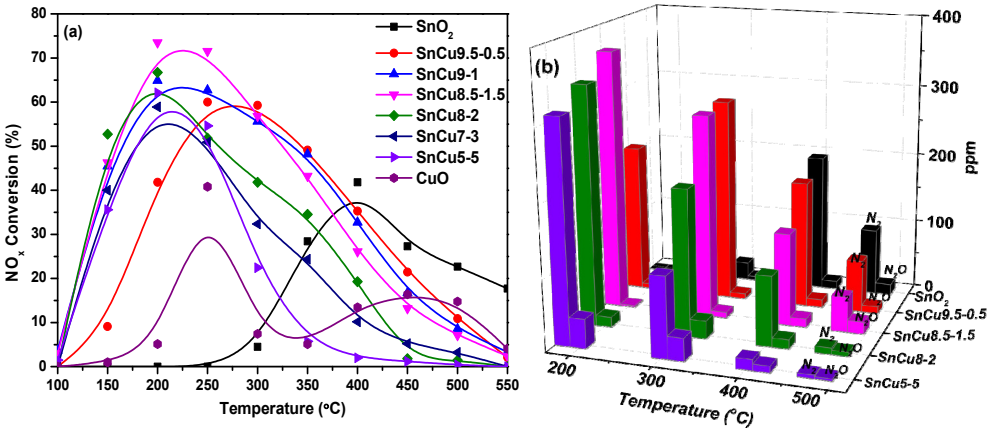

Fig. 3. Selective reduction of NO_x with NH_3 on the catalysts. (a) NO_x conversion; (b) N_2 and N_2O concentrations.

al metal oxides in spite of the Sn/Cu ratio. In particular, for SnCu9.5–0.5, SnCu9–1, SnCu8.5–1.5, the three catalysts consisting of a pure solid solution phase, the NO_x conversion kept increasing and shifted to a lower-temperature region with increasing in the amount of lattice Cu^{2+} cations. In addition, the NO_x conversion windows of the three samples become significantly wider. SnCu8.5–1.5, the sample with a Cu content close to the lattice capacity, provided the best reaction performance, with a highest NO_x conversion of around 70% achieved at a temperature as low as 200 °C and a wide temperature window. When the Cu content was above the lattice capacity, starting from SnCu8–2, the reaction performance kept deteriorating with increase in the Cu content, which demonstrated that the CuO species formed on the catalyst surface was in fact harmful to the reaction performance.

Taking into account the results obtained, it was concluded that an evident lattice capacity effect was also present in NO_x-SCR with NH_3 over Sn–Cu binary oxide catalysts, which is believed to be closely related to the change in structure induced by the varied Cu contents. A Sn–Cu catalyst with the best reaction performance can be obtained by forming the largest amount of solid solution by introducing Cu^{2+} cations into the SnO_2 lattice at a quantity close to the lattice capacity [22,23].

3.5. H_2-TPR and O_2-TPD analysis of catalysts

To investigate the redox behavior of the catalysts, H_2-TPR experiments were undertaken, and the profiles are shown in Fig. 4. Pure SnO_2 shows a major reduction peak at 621 °C, ascribed to the reduction of Sn^{4+} to metallic Sn^0 [36]. Pure CuO shows a major reduction peak at 278 °C, assigned to the reduction of Cu^{2+} to metallic Cu^0 [37]. For the Sn–Cu binary oxide catalysts, three groups of reduction peaks can be distinctly observed below 280 °C, around 330 °C, and above 400 °C. The multiple reduction peaks below 280 °C can be attributed to the stepwise reduction of Cu^{2+} cations having different chemical environments [20]. In contrast, the reduction peak above 400 °C can be assigned to the reduction of SnO_2 to metallic Sn [20], as also confirmed by the quantification of the O/Sn atomic ratio at 2.0 (Table 4). For the Sn–Cu oxide catalysts, the reduction peaks shifted to lower temperatures, demonstrating that the lattice oxygen becomes more facile and reducible. Moreover, for all the Sn–Cu oxide catalysts, a further small reduction peak at around 330 °C was detected, which can be clearly observed in the enlarged profile shown in Fig. 4(b), which corresponds to the reduction of the deficient oxygen species of SnO_2 [38]. It has been previously reported that, in a SnO_2 sample calcined below 400 °C with lower crystallinity, this deficient oxygen species is present and can be detected by H_2-TPR [39]. However, when the calcination temperature is over 400 °C, this type of facile oxygen species is depleted. On introducing Cu^{2+} cations into the SnO_2 lattice to form a solid solution structure, this deficient oxygen species of SnO_2 is effectively stabilized [40].

Furthermore, Table 4 shows that SnCu9–1 and SnCu8.5–1.5, the catalysts with a pure solid solution phase, possessed a larger number of surface deficient oxygen than other Sn–Cu oxide catalysts and pure SnO_2, in agreement with the Raman results. As a consequence, the two catalysts exhibited a much improved reaction performance, as shown in Fig. 3.

O_2-TPD was performed to further determine the facile nature of the oxygen of the Sn–Cu binary oxide catalysts, and the profiles are shown in Fig. S2. Pure SnO_2 showed two small peaks centered at ~85 °C and ~400 °C, which correspond to the desorption of facile surface oxygen and surface lattice oxygen, respectively. Pure CuO showed no detectable O_2 desorp-

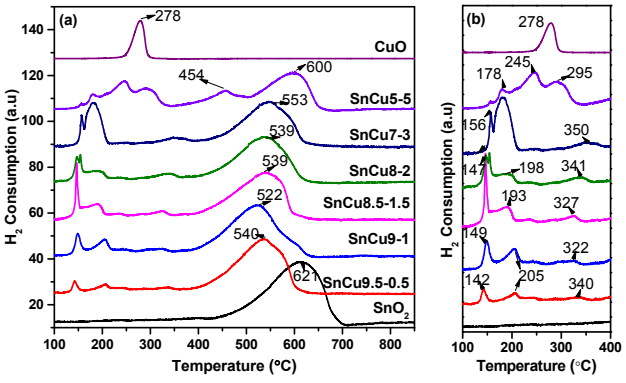

Fig. 4. H_2-TPR profiles of the catalysts. (a) complete profiles; (b) partly enlarged profiles.

Table 4
H_2-TPR results for the catalysts.

Catalyst	H_2 uptake amount of deficient oxygen below 400 °C (mmol $g_{cat}^{-1} \times 10^{-2}$) [a]	H_2 uptake amount of lattice oxygen above 400 °C		O/Sn atomic ratio [b]
		mmol g_{cat}^{-1}	mmol g_{SnO2}^{-1}	
SnO_2	1.5	13.2	13.2	2.0
SnCu9.5–0.5	7.8	12.2	13.2	2.0
SnCu9–1	13.2	11.7	13.2	2.0
SnCu8.5–1.5	13.5	11.0	13.2	2.0
SnCu8–2	13.1	10.2	13.2	2.0
SnCu7–3	10.2	9.8	13.2	2.0
SnCu5–5	3.2	8.9	13.2	2.0

[a] Quantified H_2 uptake of the deficient oxygen by excluding contribution from Cu^{2+} reduction.
[b] Calculated from H_2 reduction peak above 400 °C.

tion peak in this temperature region. In contrast, all the Sn–Cu oxide catalysts exhibited multiple oxygen desorption peaks. For easy comparison, the peaks have been classified into two categories [21]. The peak below 250 °C is labeled as α type and the peak above 250 °C is labeled as β type. As indicated by the quantification results summarized in Table 5, compared with pure SnO_2, the integrated areas of the α peak for all Sn–Cu oxide catalysts improved significantly, demonstrating the generation of larger quantities of loosely bonded surface oxygen species. In addition, the integrated areas of the β peak for SnCu9.5–0.5, SnCu9–1, and SnCu8.5–1.5, the catalysts with a pure solid solution phase, also increases in comparison with that of pure SnO_2, proving the generation of a larger amount of facile surface lattice oxygen species due to the doping of Cu^{2+} cations into the SnO_2 lattice. As a consequence, all the Sn–Cu binary oxide catalysts possessed larger quantities of total active oxygen than that in pure SnO_2, which might be one of the major reasons that all the Sn–Cu binary catalysts offered better reaction performance than the unmodified SnO_2.

It is worth noting here that, similar to Raman and H_2-TPR results, an evident lattice capacity effect was also observed in O_2-TPD experiments. When the Cu content was below the lattice capacity, both the quantities of α- and β-type active oxygen increased on increasing the lattice Cu^{2+} cation amount in the order SnCu9.5–0.5 < SnCu9–1 < SnCu8.5–1.5. However, when the Cu content was above the lattice capacity, the amount of the active oxygen kept decreasing in the order SnCu8–2 > SnCu7–3 > SnCu5–5. SnCu8.5–1.5, the catalyst that had a Cu content close to the lattice capacity and formed the largest amount of the solid solution phase, clearly exhibited the largest number of active oxygen species, thus displaying the best reaction performance.

Table 5
O_2-TPD quantification results for the catalysts.

Catalyst	Oxygen desorption amount (a.u.)		Total amount (a.u.)
	α peak (below 250 °C)	β peak (above 250 °C)	
SnO_2	4	17	21
SnCu9.5–0.5	13	19	32
SnCu9–1	57	32	89
SnCu8.5–1.5	60	40	100
SnCu8–2	46	14	60
SnCu7–3	42	—	42
SnCu5–5	37	—	37
CuO	—	—	—

To clearly demonstrate the role of active oxygen in the NO_x-SCR reaction, the relationship between the total active oxygen amount and NO_x conversion at 200 and 300 °C are shown in Fig. 5. NO_x conversion clearly rose with increase in the total active oxygen amount, demonstrating that the active oxygen species is one of major factors deciding the activity of the Sn–Cu binary oxide catalysts, which probably facilitates NO oxidation into NO_2, a key step for the reaction [24].

3.6. NH_3-TPD analysis of acidic sites on catalyst surfaces

It has been reported previously that surface acidic sites can adsorb and activate NH_3 molecules, which is a crucial step in NO_x-SCR with NH_3 [34,41]. Hence, NH_3-TPD experiments were conducted to determine the surface acidity of the catalysts, and the profiles are shown in Fig. S3. For easy comparison, the desorption peaks have been classified into three categories based on the temperature difference. The α peak below 250 °C can be assigned to NH_3 adsorbed on weak acidic sites, the β peak between 250 and 450 °C can be attributed to NH_3 adsorbed on acidic sites with moderate strength, and the γ peak above 450

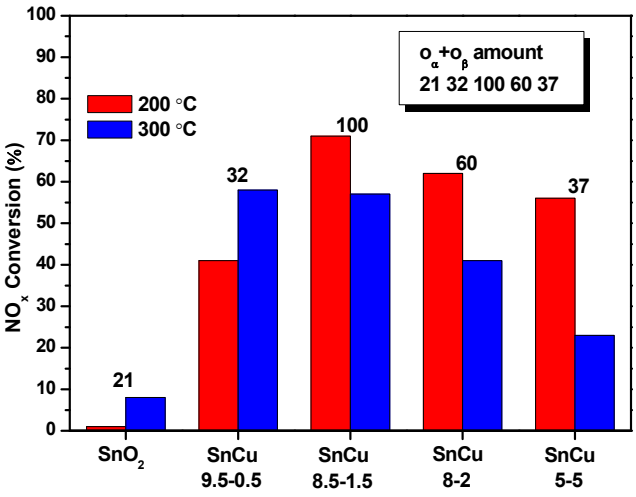

Fig. 5. NO_x conversion on the catalysts at 200 and 300 °C against total active oxygen amount obtained with O_2-TPD.

Table 6
NH_3-TPD quantification results for the catalysts.

Catalyst	NH_3 desorption amount (a.u.)			Total amount (a.u.)
	α peak (below 250 °C)	β peak (250–400 °C)	γ peak (above 450 °C)	
SnO_2	3	1	2	6
SnCu9.5–0.5	2	27	—	29
SnCu9–1	3	42	30	75
SnCu8.5–1.5	27	54	19	100
SnCu8–2	17	57	10	84
SnCu7–3	13	51	16	80
SnCu5–5	35	34	8	77
CuO	0	23	0	23

°C can be ascribed to NH_3 adsorbed on strong acidic sites [42]. According to the quantification results summarized in Table 6, the NH_3 desorption amount on Sn–Cu binary oxide catalysts improved significantly in comparison with that on pure SnO_2 and CuO, suggesting the formation of much larger numbers of surface acidic sites. Since the reaction results suggested a wide range of NO_x conversion values for the temperature range of 100–450 °C, we believe that all the acidic sites participated in the reaction at different temperatures. Therefore, for clarification, the relationship between the total NH_3 desorption amount and NO_x conversion determined at 200 and 300 °C has been plotted in Fig. 6. It is apparent that a catalyst with a larger number of acidic sites exhibits better reaction performance, which strongly suggests that the surface acidity is another crucial factor that determines the NO_x-SCR performance on Sn–Cu binary catalysts. It is worth noting here that the same lattice capacity effect as that suggested by Raman, H_2-TPR, and O_2-TPD results were also observed in the NH_3-TPD investigation, which again confirmed that the best reaction performance can be achieved by forming the largest amount of Sn–Cu pure solid solution phase.

3.7. SO_2 and water vapor resistance of catalysts

SnCu8.5–1.5, the catalyst with a Cu content close to the lattice capacity, showed the best reaction performance among all the Sn–Cu binary oxide catalysts due to the presence of the largest numbers of surface facile oxygen and surface acidic sites. To explore its application potential, the stability of SnCu8.5–1.5 was tested at 200 °C in the presence of water vapor or/and SO_2, which are usually present in most exhausts of diesel engines [43]. As shown in Fig. 7, after the NO_x conversion stabilized at ~73% for 10 h, the introduction of 5% water vapor into the reaction feed decreased the NO_x conversion to ~35%, but the conversion could be completely recovered after removing the water vapor. After stabilization for another 10 h, the introduction of 0.01% SO_2 in the reaction feed decreased 5% NO_x conversion, but the conversion could, again, be regenerated after removing the SO_2. When 0.005% SO_2 and 5% water vapor were added into the reaction feed together, the NO_x conversion dropped significantly to 20%, indicating that the coexistence of both poisoning species had a more severe negative impact on the reaction performance. However, after both were removed from the gas feed, the NO_x conversion could be recovered to ~70%, which was slightly lower than the initial NO_x conversion obtained on the fresh catalyst. These results demonstrated that either SO_2 or water vapor alone has no permanent influence on the structure of the SnCu8.5–1.5 catalyst but merely occupy some surface active sites temporarily but if both coexist in the gas feed, then some permanent deactivation might occur slowly, possibly due to the formation of sulfuric acid. In summary, SnCu8.5–1.5 displayed appreciable resistance to both SO_2 and water vapor. With further optimization, Sn–Cu solid solution catalysts could offer better reaction performance and stability.

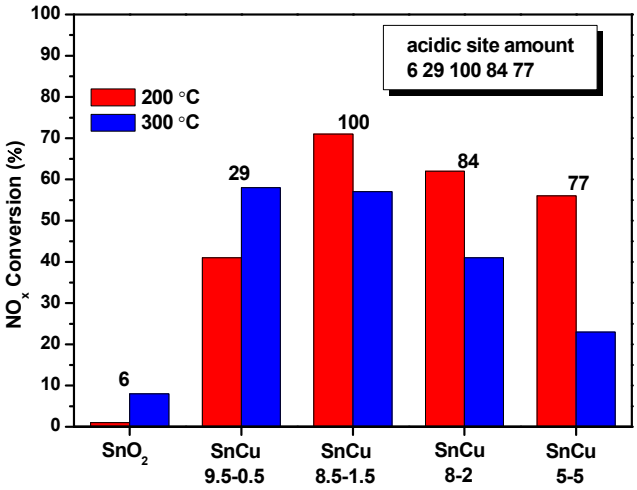

Fig. 6. NO_x conversion on the catalysts at 200 and 300 °C against total acidic site determined by NH_3-TPD.

4. Conclusions

With the objective to understand the effect of the doping amount of Cu^{2+} on the structure and reactivity of SnO_2 for NO_x-SCR with NH_3, a series of Sn–Cu–O binary oxide catalysts with different Sn/Cu ratios was prepared by the coprecipitation method and thoroughly characterized.

Using the XRD extrapolation method, the SnO_2 lattice capacity for Cu^{2+} cations was quantified to be 0.10 g CuO per g SnO_2,

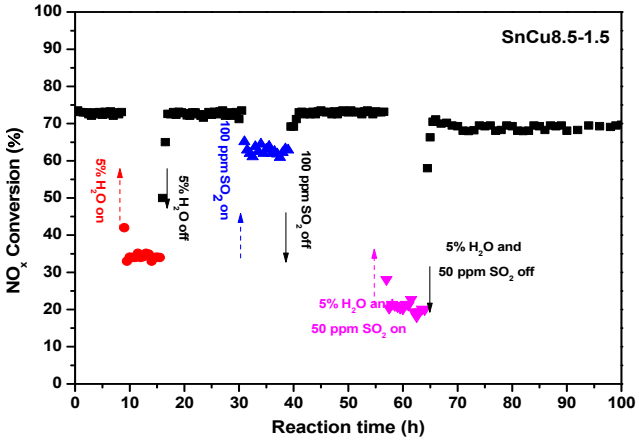

Fig. 7. Stability test of SnCu8.5–1.5 in the presence of H_2O or/and SO_2 for NO_x-SCR with NH_3 at 200 °C.

equaling a Sn/Cu molar ratio of 84/16. If the Cu content was above the lattice capacity, CuO species will start to form on the catalyst surface, which negatively affects the reaction performance.

In the samples with Cu contents not exceeding the lattice capacity, Cu was present completely as Cu^{2+} cations in the SnO_2 lattice, forming a pure solid solution phase. On increasing the Cu content, Raman results confirmed that the amount of surface defects increased until the lattice capacity was reached. H_2-TPR, O_2-TPD, and NH_3-TPD results proved that both the numbers of surface active oxygen sites and acidic sites, which critically determine the reaction performance, also increased for these catalysts and reached the maximum values for the catalyst with a Cu content close to the lattice capacity.

A distinct lattice capacity threshold effect on the structure and reactivity of Sn–Cu binary oxide catalysts has thus been demonstrated. A Sn–Cu catalyst with the best reaction performance for NO_x-SCR with NH_3 can be achieved by doping the SnO_2 matrix with the lattice capacity amount of Cu^{2+} cations, so that the largest amount of pure phase solid solution is formed, as well as the numbers of surface active oxygen species and acidic sites are maximized.

References

[1] P. Granger, V. I. Parvulescu, *Chem. Rev.*, **2011**, 111, 3155–3207.
[2] D. Damma, P. R. Ettireddy, B. M. Reddy, P. G. Smirniotis, *Catalysts*, **2019**, 9, 349.
[3] J. Xu, G. Chen, F. Guo, J. Xie, *Chem. Eng. J.*, **2018**, 353, 507–518.
[4] X. Huang, G. Zhang, G. Lu, Z. Tang, *Catal. Surv. Asia.*, **2018**, 22, 1–19.
[5] J. Li, Y. Peng, H. Chang, X. Li, J. C. Crittenden, J. Hao, *Front. Environ. Sci. Eng.*, **2016**, 10, 413–427.
[6] J. Wang, H. Zhao, G. Haller, Y. Li, *Appl. Catal. B*, **2017**, 202, 346–354.
[7] C. Tang, H. Zhang, L. Dong, *Catal. Sci. Technol.*, **2016**, 6, 1248–1264.
[8] C. Liu, J.-W. Shi, C. Gao, C. Niu, *Appl. Catal. A*, **2016**, 522, 54–69.
[9] J. Li, H. Chang, L. Ma, J. Hao, R. T. Yang, *Catal. Today*, **2011**, 175, 147–156.
[10] W.-T. Chen, K.-B. Chen, M.-F. Wang, S.-F. Weng, C.-S. Lee, M. C. Lin, *Chem. Commun.*, **2010**, 46, 3286–3288.
[11] J. Sun, Y. Lu, Z. Lei, C. Ge, C. Tang, H. Wan, D. Lin, *Ind. Eng. Chem. Res.*, **2017**, 56, 12101–12110.
[12] J. Y. Wei, Y. X. Zhu, L. Y. Duan, Y. C. Xie, *Chin. J. Catal.*, **2003**, 24, 414–418.
[13] X. Yao, C. Tang, Z. Ji, Y. Dai, Y. Cao, F. Gao, L. Dong, Y. Chen, *Catal. Sci. Technol.*, **2013**, 3, 688–698.
[14] P. Zhang, H. Lu, Y. Zhou, L. Zhang, Z. Wu, S. Yang, H. Shi, Q. Zhu, Y.

Graphical Abstract

Chin. J. Catal., 2020, 41: 877–888 doi: 10.1016/S1872-2067(20)63532-X

Investigation of lattice capacity effect on Cu^{2+}-doped SnO_2 solid solution catalysts to promote reaction performance toward NO_x-SCR with NH_3

Xianglan Xu, Yunyan Tong, Jingyan Zhang, Xiuzhong Fang, Junwei Xu, Fuyan Liu, Jianjun Liu, Wei Zhong, Olga E. Lebedeva, Xiang Wang *
Nanchang University, China; Jiangxi Baoan New Material Technology Corporation, LTD, China; Jiaxing University, China; Belgorod State National Research University, Russian Federation

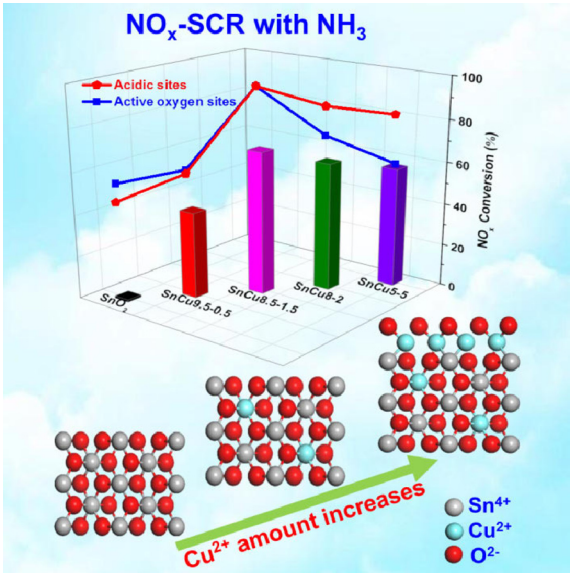

Doping the SnO_2 matrix with the lattice capacity amount of Cu^{2+} gives an optimal Sn–Cu catalyst for NO_x-SCR with NH_3 by maximizing surface active oxygen and acidic sites.

Chen, S. Dai, *Nat.Commun.*, **2015**, 6.
[15] X. Yao, Y. Xiong, W. Zou, L. Zhang, S. Wu, X. Dong, F. Gao, Y. Deng, C. Tang, Z. Chen, L. Dong, Y. Chen, *Appl. Catal. B*, **2014**, 144, 152–165.
[16] D. Devaiah, L. H. Reddy, S.-E. Park, B. M. Reddy, *Catal. Rev. Sci. Eng.*, **2018**, 60, 177–277.
[17] M. Sugiura, *Catal. Surv. Asia.*, **2003**, 7, 77–87.
[18] C. Liu, H. Xian, Z. Jiang, L. Wang, J. Zhang, L. Zheng, Y. Tan, X. Li, *Appl. Catal. B*, **2015**, 176, 542–552.
[19] Z. Liu, X. Feng, Z. Zhou, Y. Feng, J. Li, *Appl. Surf. Sci.*, **2018**, 428, 526–533.
[20] Y. Li, H. Peng, X. Xu, Y. Peng, X. Wang, *RSC Adv.*, **2015**, 5, 25755–25764.
[21] Y. Liu, Y. Guo, Y. Liu, X. Xu, H. Peng, X. Fang, X. Wang, *Appl. Surf. Sci.*, **2017**, 420, 186–195.
[22] Q. Sun, X. Xu, H. Peng, X. Fang, W. Liu, J. Ying, F. Yu, X. Wang, *Chin. J. Catal.*, **2016**, 37, 1293–1302.
[23] X. Xu, F. Liu, X. Han, Y. Wu, W. Liu, R. Zhang, N. Zhang, X. Wang, *Catal. Sci. Technol.*, **2016**, 6, 5280–5291.
[24] J. Zhang, Y. Liu, Y. Sun, H. Peng, X. Xu, X. Fang, W. Liu, J. Liu, X. Wang, *Ind. Eng. Chem. Res.*, **2018**, 57, 10315–10326.
[25] W. Hume-Rothery, G. V. Raynor, *The Structure of Metals and Alloys*, Institute of Metals, London, **1962**.
[26] Y. Zhang, Y. J. Zhou, J. P. Lin, G. L. Chen, P. K. Liaw, *Adv. Eng. Mater.*, **2008**, 10, 534–538.
[27] R. Craciun, B. Nentwick, K. Hadjiivanov, H. Knözinger, *Appl. Catal. A*, **2003**, 243, 67–79.
[28] A. Denton, N. W. Ashcroft, *Phys. Rev. A*, **1991**, 43, 3161–3164.
[29] A. Diéguez, A. Romano-Rodríguez, A. Vilà, J. R. Morante, *J. Appl. Phys.*, **2001**, 90, 1550–1557.
[30] V. Bonu, A. Das, A. K. Sivadasan, A. K. Tyagi, S. Dhara, *J. Raman. Spectrosc.*, **2015**, 46, 1037–1040.
[31] W. Ben Haj Othmen, B. Sieber, H. Elhouichet, A. Addad, B. Gelloz, M. Moreau, S. Szunerits, R. Boukherroub, *Mater. Sci. Semicon. Proc.*, **2018**, 77, 31–39.
[32] W. Wang, L. Wang, H. Shi, Y. Liang, *CrystEngComm.*, **2012**, 14, 5914–5922.
[33] H. Siddiqui, M. S. Qureshi, F. Z. Haque, *Optik.*, **2016**, 127, 3713–3717.
[34] Y. Xiong, C. Tang, X. Yao, L. Zhang, L. Li, X. Wang, Y. Deng, F. Gao, L. Dong, *Appl. Catal. A*, **2015**, 495, 206–216.
[35] J. Chen, Y. Chen, M. Zhou, Z. Huang, J. Gao, Z. Ma, J. Chen, X. Tang, *Environ. Sci. Technol.*, **2017**, 51, 473–478.
[36] C. Rao, J. Shen, F. Wang, H. Peng, X. Xu, H. Zhan, X. Fang, J. Liu, W. Liu, X. Wang, *Appl. Surf. Sci.*, **2018**, 435, 406–414.
[37] J. Shen, C. Rao, Z. Fu, X. Feng, J. Liu, X. Fan, H. Peng, X. Xu, C. Tan, X. Wang, *Appl. Surf. Sci.*, **2018**, 453, 204–213.
[38] M. Batzill, U. Diebold, *Prog. Surf. Sci.*, **2005**, 79, 47–154.
[39] R. Sasikala, N. M. Gupta, S. K. Kulshreshtha, *Catal. Lett.*, **2001**, 71, 69–73.
[40] M. A. Mäki-Jaskari, T. T. Rantala, *Phys. Rev. B.*, **2002**, 65, 245428/1–245428/8.
[41] C. Liu, L. Chen, J. Li, L. Ma, H. Arandiyan, Y. Du, J. Xu, J. Hao, *Environ. Sci. Technol.*, **2012**, 46, 6182–6189.
[42] Y. Peng, W. Si, X. Li, J. Chen, J. Li, J. Crittenden, J. Hao, *Environ. Sci. Technol.*, **2016**, 50, 9576–9582.
[43] Y. Jangjou, D. Wang, A. Kumar, J. Li, W. S. Epling, *ACS Catal.*, **2016**, 6, 6612–6622.

Cu^{2+}离子掺杂SnO_2固溶体催化剂的晶格容量效应: NH_3选择性还原NO_x反应性能提高的本质原因

徐香兰[a], 佟云艳[a], 张景岩[a], 方修忠[a], 徐骏伟[a], 刘福燕[a], 刘建军[b], 钟　伟[c], Olga E. Lebedeva[d], 王　翔[a,*]

[a]南昌大学化学学院, 江西省环境与能源催化重点实验室, 江西南昌330031, 中国
[b]江西宝安新材料科技有限公司, 江西萍乡337000, 中国
[c]嘉兴学院生物与化学工程学院, 浙江嘉兴314001, 中国
[d]贝尔哥罗德国家研究大学, 贝尔哥罗德, 俄罗斯

摘要: NO_x排放给人类健康和环境带来了严重的危害, 目前已发展了多种消除其污染的方法. 其中氨选择性催化还原(NH_3-SCR)技术是固定源和移动源柴油机排放NO_x的有效消除方法之一. 非贵金属氧化物催化剂由于廉价、且原料来源丰富, 用于NH_3-SCR反应在过去几十年一直备受人们关注. 由于晶格畸变和不等价取代等原因, 与单组分氧化物催化剂相比, 替代型金属氧化物固溶体催化剂通常具有更优异的物理化学性能. 其中典型的例子是已被广泛用作汽车尾气净化转化器储氧材料的铈锆固溶体. 与纯CeO_2相比, Zr^{4+}离子溶入立方萤石CeO_2晶格形成固溶体结构后, 显著提高了其稳定性和储氧能力. 近八年来, 我们以四方金红石型SnO_2为溶剂, 系统地研究了系列金属阳离子在其晶格中的溶解行为, 并考察了其催化反应性能. 为深入理解固溶体催化剂的结构与反应性能之间的关系, 我们首次创建了简单易行的XRD外推法定量金属氧化物固溶体中溶质阳离子的晶格容量. 结果表明, 其它离子掺杂形成SnO_2基固溶体可显著增加其表面缺位氧和Lewis酸性位点的数量, 且可使缺位氧在较高温度下保持稳定, 显著提高了所得催化剂的反应性能. 另外我们还发现, 当溶质离子含量为晶格容量时可得到最大量的纯相固溶体, 此时催化剂通常具有最优的性能, 具有明显的阈值效应.

很多研究表明, 含CuO的一些催化材料通常对NO_x选择还原具有良好的低温活性和选择性, 但把Cu^{2+}离子溶入SnO_2晶格构建固溶体催化剂用于NH_3-SCR反应迄今未见报道. 因此, 为获得性能优良的催化剂, 本文采用共沉淀法制备了系列不同Cu^{2+}离子含量的Sn-Cu复合氧化物固溶体催化剂, 并采用XRD外推法测定了Cu^{2+}离子在SnO_2中的晶格容量, 为0.10 g CuO /g SnO_2, 相当于Sn/Cu摩尔比为84/16. Raman结果表明, Cu^{2+}离子含量低于晶格容量时, 随其含量增加, 表面氧缺位数量增加, 且在晶格容量时达到最大. H_2-TPR, O_2-TPD和NH_3-TPD结果表明, 随着Cu^{2+}离子含量增加, 催化剂表面活性氧物种和表

面酸中心的数量均增加; 在Cu^{2+}离子含量接近晶格容量时, 催化剂中形成最大量的纯固溶体相, 上述活性中心均可达到最大量. 此时, 催化剂具有最佳的NH_3-SCR反应性能. 因此, Cu^{2+}离子溶入SnO_2晶格形成固溶体催化剂, 在结构和反应性能上均具有明显的晶格容量阈值效应. 通过将Cu^{2+}离子含量调控在晶格容量, 可获得反应性能最好的Sn-Cu复合氧化物固溶体催化剂.

关键词: SnO_2基固溶体; Cu^{2+}离子晶格容量; XRD外推法; NO_x的NH_3选择还原; 晶格容量阈值效应

收稿日期: 2019-11-13. 接受日期: 2019-12-10. 出版日期: 2020-05-05.

*通讯联系人. 电话: 15979149877; 电子信箱: xwang23@ncu.edu.cn

基金来源: 国家自然科学基金(21567016, 21666020, 21962009); 江西省自然科学基金(20181ACB20005, 20171BAB213013); 江西省环境与能源催化重点实验室(20181BCD40004); 国家重点研发计划(2016YFC0209302); 江西省研究生创新基金(YC2018-B015); 浙江省自然科学基金(LY18B010007).

本文的电子版全文由Elsevier出版社在ScienceDirect上出版(http://www.sciencedirect.com/science/journal/18722067).